The Measured Equation of Invariance Method Applied to Randomly Rough Surfaces

John B. Schneider and Shira Lynn Broschat*

Abstract

The Measured Equation of Invariance (MEI) method has received considerable attention recently. Unlike more traditional numerical techniques, MEI solutions are obtained by inversion of a relatively small *and* sparse matrix. Therefore, the MEI method can potentially provide a solution much more quickly than other techniques. To date, the MEI method has been applied primarily to discrete objects. In this paper, bistatic radar cross sections for one-dimensional, perfectly conducting, randomly rough surfaces are obtained using the MEI method. The implementation suitable for this problem requires some modification and enhancement of the original algorithm to achieve the desired accuracy. These algorithmic changes can be applied to the discrete scattering problem as well. Monte Carlo results for the bistatic scattering cross section for surfaces with Gaussian statistics and satisfying a Gaussian roughness spectrum are compared to those from another technique and excellent agreement is obtained.

I. Introduction

The Measured Equation of Invariance (MEI) method was recently introduced [1, 2, 3, 4] as a way to determine the electromagnetic fields scattered from discrete objects. Initially, results were reported mostly for conducting two-dimensional objects, but the method can be applied much more broadly. Hybrid techniques have been used in conjunction with the MEI method to obtain scattering from penetrable objects [5, 6, 7, 8]; however, many of these scatterers can be analyzed using a simpler scheme if the metrons are selected carefully [2]. Additionally, the MEI method can be used to provide solutions to Laplace's equation [3, 9].

The principal attraction of the MEI method is that it yields a solution via a sparse and relatively small matrix, and hence requires much less time and memory than more conventional techniques. The computational mesh is terminated very close to the scattering object. Interior mesh points are related to each other using standard finite difference techniques while boundary nodes are handled using the Measured Equations of Invariance. The time required to fill the matrix is roughly $O(N^2)$, where N is the number of unknowns on the boundary. Because the matrix is sparse, the time required to invert the matrix is small ($O(N)$); thus, the total computation time is dominated by the time required to fill the matrix. This is in contrast to the traditional Method of Moments approach which requires the inversion of a full matrix (an $O(N^3)$ operation).

In this paper the MEI method is used to solve for the bistatic radar cross sections for randomly rough surfaces. Specifically, ensemble averaging over a number of surface realizations is used to approximate the results for a single, infinitely long surface. Surfaces with Gaussian statistics and satisfying a Gaussian roughness spectrum are assumed. However, it should be emphasized that this numerical technique is not restricted to this class of surfaces.

In Section II a brief review of the MEI method is provided. The pertinent aspects of the rough surface scattering problem are outlined in Section III. In Section IV our implementation of a MEI-based solution to the problem is described. Finally, results are presented in Section V.

II. Review of the MEI Method

Ultimately, our goal is to solve the wave equation subject to the appropriate boundary conditions. For the

*The authors are with the School of Electrical Engineering and Computer Science, Washington State University, Pullman, WA 99164-2752

sake of concreteness, we assume TM illumination of a perfectly-conducting, two-dimensional scatterer (e.g., a surface for which the height varies as a function of one spatial coordinate) so that the governing differential equation is reduced to a scalar one:

$$(\nabla^2 + k^2)E_z = 0 \tag{1}$$

where k is the wavenumber of the incident field. If space is discretized into a uniform mesh and a local configuration of nodes is as shown in Fig. 1, (1) can be approximated using central differences to obtain

$$-(4 - k^2\Delta^2)E_{z0} + E_{z1} + E_{z2} + E_{z3} + E_{z4} = 0 \tag{2}$$

where Δ is the separation between mesh points. This can be written more generally as

$$\sum_{i=0}^{N} \alpha_i E_{zi} = 0, \tag{3}$$

where N is the number of nodes "connected" to the zeroth (central) node and the α_i's represent appropriate weights. For a Cartesian structure, such as in Fig. 1, all weights for the surrounding nodes are equal. Had a polar mesh been used, the weights would have to account for the global location within the mesh, i.e., the weights would be a function of the radial distance from the origin. If a higher-order differencing scheme had been used, N would have to be increased. These difference equations are invariant to the location and geometry of the scatterer and to the field of excitation. The appeal of the finite difference formulation is the sparsity and ease of calculating the non-zero elements in the resulting matrix. However, the finite difference approach is problematic in that it provides no simple way to terminate the computational mesh for unbounded problems.

To address this shortcoming, Mei developed the Measured Equation of Invariance (MEI) method that combines features of both differential and integral based methods [4]. Basically, the MEI method provides a means to select appropriate α_i's in (3) so that the mesh need not be orthogonal. This allows the fields at the nodes on the edge of the computational domain to be related simply to points in the interior. Furthermore, Mei maintains that the resulting set of equations (and hence the α_i's) is location dependent, geometry specific, and invariant to the field of excitation. The MEI method does not seek to find a strict discretization of the wave equation. Instead, the discretization that is obtained is an approximation to an unknown operator that satisfies both the wave equation and the radiation condition. This is discussed in more detail in [2].

To illustrate the technique, consider the configuration of nodes shown in Fig. 2. These nodes are typical of the mesh at the edge of the computational domain. We seek α_i's such that

$$\sum_{i=0}^{3} \alpha_i E_{zi} = 0. \tag{4}$$

Since (4) is a homogeneous equation, one of the weights (e.g., α_0) may be chosen arbitrarily. The remaining three weights are determined via three equations. These equations are obtained by assuming independent source distributions, known as metrons, over the surface of the scatterer. Each metron gives rise to a field, known as the measured field, which is easily calculated. The weights are obtained by satisfying (4) for each of the measured fields. Specifically, three metrons are assumed J_s^1, J_s^2, and J_s^3. From these the nth measured field $E_z^n(\mathbf{r})$ is obtained via

$$E_z^n(\mathbf{r}) = \int_S J_s^n(\mathbf{r}')G(\mathbf{r}|\mathbf{r}')ds' \tag{5}$$

where $\mathbf{r}$ is the observation point, $\mathbf{r}'$ is a point on the surface, and $G(\mathbf{r}|\mathbf{r}')$ is the appropriate Green's function (typically the free space Green's function). Assuming $\alpha_0 = 1$, the remaining weights are obtained using

$$\begin{bmatrix} \alpha_1 \\ \alpha_2 \\ \alpha_3 \end{bmatrix} = - \begin{bmatrix} E_{z1}^1 & E_{z2}^1 & E_{z3}^1 \\ E_{z1}^2 & E_{z2}^2 & E_{z3}^2 \\ E_{z1}^3 & E_{z2}^3 & E_{z3}^3 \end{bmatrix}^{-1} \cdot \begin{bmatrix} E_{z0}^1 \\ E_{z0}^2 \\ E_{z0}^3 \end{bmatrix} \tag{6}$$

which can be written as

$$\boldsymbol{\alpha} = -\mathbf{M}^{-1} \cdot \mathbf{M}_0 \tag{7}$$

where the matrix $\mathbf{M}$ contains the measured fields at the neighboring nodes while the vector $\mathbf{M}_0$ contains the fields sampled at the zeroth node.

Although the metrons are chosen to be independent, the sampled values of the measured fields over a small number of mesh points may not be independent. Hence, the matrix $\mathbf{M}$ may be singular and a solution to (7) will not exist. There are several ways to circumvent this problem. Perhaps the easiest is to use more metrons, and subsequently more measured fields, than unknowns. In this

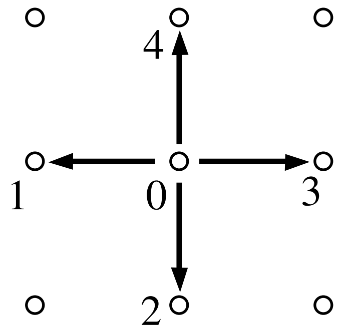

Figure 1: Nodes in the computational mesh.

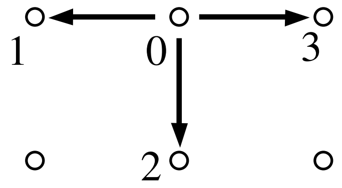

Figure 2: Typical configuration of nodes at the edge of the computational mesh

case, the weights are obtained via least squares so that $\boldsymbol{\alpha}$ is the vector that minimizes $\|\mathbf{M}\cdot\boldsymbol{\alpha}+\mathbf{M}_0\|$. This least squares operation is performed on a small matrix (e.g., in the work presented here $\mathbf{M}$ is 5×3) and thus requires neglible time relative to the calculation of the measured fields.

In principle the MEI method can be used for all nodes within the computational domain. However, this would require careful treatment of the singularity in the integrand of (5) for nodes adjacent to the surface (i.e., at least one neighboring node would be on the surface and the measured field for this node would require careful calculation of (5)). To obviate the consideration of this singularity, a layer of nodes that use standard finite difference coefficients is placed adjacent to the surface. If the mesh is non-orthogonal, but relatively undistorted, Pous has found that weights can be obtained using a local polar approximation [2]. This layer of nodes insures that the measured fields only need to be calculated at points above the surface.

From this point, the MEI method is similar to the finite difference method. The weights found above are used to construct a "connectivity matrix" $\mathbf{A}$ that specifies the relationship between every node in the mesh. Each row number corresponds to the global node number for a given unknown (i.e., the field at that node). The non-zero elements in that row correspond to the α_i's associated with the neighboring nodes and the node itself. The connectivity matrix is sparse, and it may have other structure (such as bandedness) that can be exploited. For nodes that are adjacent to the surface of the scatterer, one of the neighboring values corresponds to the known surface field which serves as the forcing function to the system of equations. Symbolically, this is written as

$$\mathbf{A}\cdot\mathbf{E}=\mathbf{F} \tag{8}$$

where $\mathbf{E}$ contains the unknown field values at each node in the computational mesh and $\mathbf{F}$ is the forcing function determined by a combination of the known surface field and the weights determined using the local polar approximation. The solution is then obtained via

$$\mathbf{E}=\mathbf{A}^{-1}\mathbf{F}. \tag{9}$$

Once $\mathbf{E}$ has been determined, the actual surface currents are deduced and far-field quantities are obtained as described in Sec. IV.

III. Rough Surface Scattering Problem

Currently rough surface scattering is of interest to researchers in a variety of disciplines. It has applications in such diverse areas as ultrasonics, radar imaging, sonar detection, solid-state physics, optics, astronomy, and microwave remote sensing.

In the past three decades, much work has been done in the development of approximate analytic models to predict wave scattering from rough surfaces. These include the small slope approximation [10, 11, 12], the phase perturbation technique [13, 14], the operator expansion method [15, 16], the Dashen-Wurmser approximation [17], the unified perturbation method [18, 19], and the quasi-slope approximation [20]. In addition, some work has been done in the development of Monte Carlo numerical techniques that are exact in the sense that no physical approximations are made in the underlying equations. These include techniques based on integral equations [21, 22], the finite element method [23], and finite difference methods [24, 25, 26]. In this work we consider the MEI method. We restrict our consideration to perfectly conducting, one-dimensional, randomly rough surfaces with Gaussian statistics and satisfying a Gaussian surface roughness spectrum [27]. Surfaces with Gaussian statistics have been studied extensively [11, 21, 28, 29].

The problem geometry is shown in Fig. 3. TM illumination is assumed so the total electric field at the surface vanishes (Dirichlet boundary condition). The surface profile is given by $f(x)$. The mean height of the surface is zero, i.e., $\langle f \rangle_s = 0$, where $\langle \cdot \rangle_s$ indicates averaging over the entire surface. The standard deviation, or RMS surface height, is given by $h = \sqrt{\langle f^2 \rangle_s}$. Both surface heights and slopes are Gaussian distributed.

The normalized correlation function is defined by

$$C(\zeta) = \frac{\langle f(x) f(x+\zeta) \rangle_s}{h^2}, \qquad (10)$$

which for Gaussian surfaces is given by

$$C(\zeta) = \exp\left(\frac{-\zeta^2}{l^2}\right). \qquad (11)$$

The correlation length l is the length at which the correlation function decreases by a factor of $1/e$. The surface roughness spectrum is obtained by taking the Fourier transform of $h^2 C(\zeta)$. For Gaussian surfaces, the statistics are completely specified by just two parameters, the correlation length and the RMS surface height, and generation of surface realizations is relatively simple [21, 27].

In numerical simulations of rough surface scattering, finite-length surfaces must be used to model scattering from infinite surfaces. When a single plane wave strikes a finite-length surface, edge diffraction occurs. One way of minimizing diffraction effects is to construct an incident wave that tapers to very small values at the surface edges. Diffraction still occurs, but it makes negligible contributions to the scattered field. Tapered incident waves have been introduced by Thorsos [21] and Chan and Fung [22]. The tapered incident field used by Thorsos is an approximation to an incident field, consisting of an angular spectrum of plane waves, that satisfies the wave equation exactly. This approximate field is given by

$$E_z^i(\mathbf{r}) = \exp\left\{-j\mathbf{k}_i \cdot \mathbf{r}\left[1 + w(\mathbf{r})\right] - (x - y\tan\theta_i)/g^2\right\} \qquad (12)$$

where

$$w(\mathbf{r}) = \left[2(x - y\tan\theta_i)^2/g^2 - 1\right]/(kg\cos\theta_i)^2, \qquad (13)$$

$\mathbf{r} = (x, y)$ is a point above the surface, θ_i is the incident angle measured from the vertical, and $\mathbf{k}_i = k_0(\sin\theta_i, \cos\theta_i)$ is the free-space incident wave vector in the xy plane. Equation (12) satisfies the wave equation to order $1/(k_0 g\cos\theta_i)^2$ for $k_0 g \cos\theta_i \gg 1$. The parameter g controls the tapering, and care must be taken in its choice. Angular resolution, edge effects, and accuracy in satisfying the wave equation all depend on g [21]. In addition, the tapering must be accomplished in such a way that differences between the finite surface, tapered plane wave results and infinite surface, single plane wave results are negligible. For the numerical examples presented in this paper, $g = L/4$ is used, where L is the horizontal extent of each surface.

For each numerical study, 50 finite-length surfaces are generated using the method proposed by Thorsos [21]. Monte Carlo results are then obtained by taking the ensemble average of the cross sections of the 50 surfaces. The general procedure is to randomly generate a surface spectrum that has Gaussian statistics and then inverse transform the spectrum to obtain a surface profile. Each surface consists of N discrete points horizontally separated by Δx over a surface length L'. The x component of each point along the surface is specified by the location $x_n = n\Delta x$ for $1 \le n \le N$. The surfaces are generated using

$$f(x_n) = \frac{1}{L'} \sum_{\ell=-N/2}^{N/2-1} F(K_\ell) \exp[-jK_\ell x_n] \qquad (14)$$

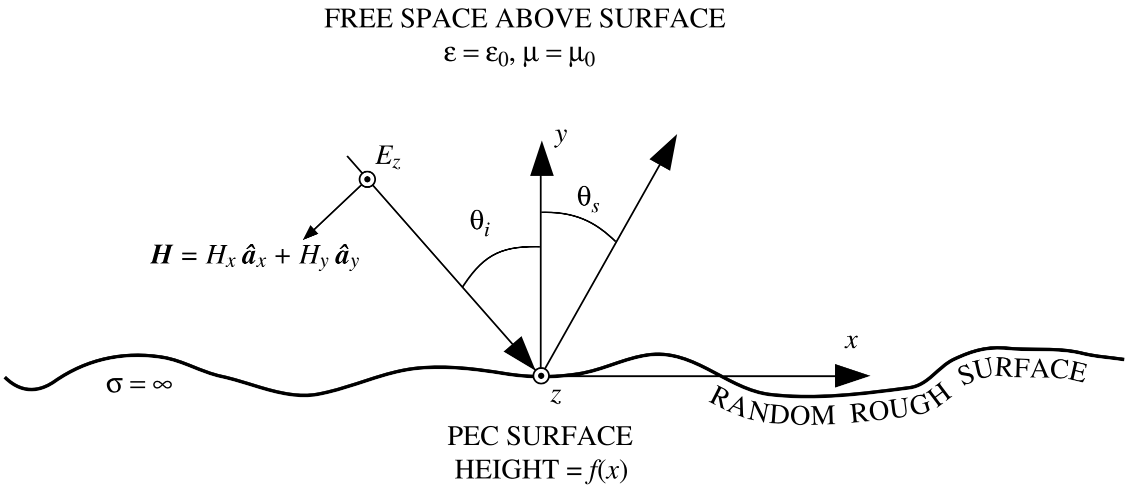

Figure 3: Problem geometry.

where, for $0 < \ell < N/2$,

$$F(K_\ell) = \sqrt{2\pi L' W(K_\ell)} \frac{1}{\sqrt{2}} [N(0,1) - jN(0,1)] \quad (15)$$

and for $\ell = 0$ or $N/2$

$$F(K_\ell) = \sqrt{2\pi L' W(K_\ell)} N(0,1) \quad (16)$$

In (14)-(16)

$$W(K_\ell) = \frac{h^2 l}{2\sqrt{\pi}} \exp[-K_\ell^2 l^2/4] \quad (17)$$

is the Gaussian surface roughness spectrum, $K_\ell = 2\pi\ell/L'$, h is the RMS surface height, l is the correlation length, and $N(0,1)$ is a number sampled from a Gaussian distribution with zero mean and unity variance. For $\ell < 0$, $F(K_{-\ell}) = F(K_\ell)^*$.

The nature of the discrete spectrum causes correlation of the ends of each surface. To circumvent this, an extended surface, several times longer than the N required points, is generated. Each surface used in the numerical simulation is then cut from the longer surface and, hence, the correlation of the ends is negligible. For the numerical studies presented here, surfaces with a length of $L' = 256\lambda$ were generated but segments of length $L = 80\lambda$ were used in the calculations (λ is the wavelength of the illumination).

IV. MEI Method for Rough Surfaces

In order to use the MEI method, a computational mesh enclosing the scattering object must be specified. Figure 4 shows a segment of a typical surface with a two-layer computational mesh. To generate the mesh, two mesh points are specified for each surface point. Both points are along the surface normal and are separated by a distance Δv. To obtain the surface normal, the surface slope is needed. The x and y components of the surface unit normal vector are

$$n_x = \frac{-f'(x)}{\sqrt{1 + [f'(x)]^2}} \quad (18)$$

$$n_y = \frac{1}{\sqrt{1 + [f'(x)]^2}} \quad (19)$$

where $f'(x) = df/dx$. The surface derivative could be obtained approximately using finite differences; however, the surface spectrum is needed to generate the surface realizations and is available to obtain surface slopes (see (14)). Thus, we find $f'(x)$ via

$$f'(x) = \mathcal{F}^{-1}(jKF(K)) \quad (20)$$

where $\mathcal{F}^{-1}$ denotes the inverse Fourier transform.

Note that the surface generation scheme creates points that are *horizontally* offset from neighboring points by Δx. However, since neighboring points do not necessarily have the same vertical components, the distance between points is nonuniform.

Figure 5 shows an expanded view of one corner of the computational mesh. The global node numbers are shown together with some of the node interconnections. Odd-numbered nodes correspond to nodes in the interior while even-numbered nodes are on the outer boundary. The

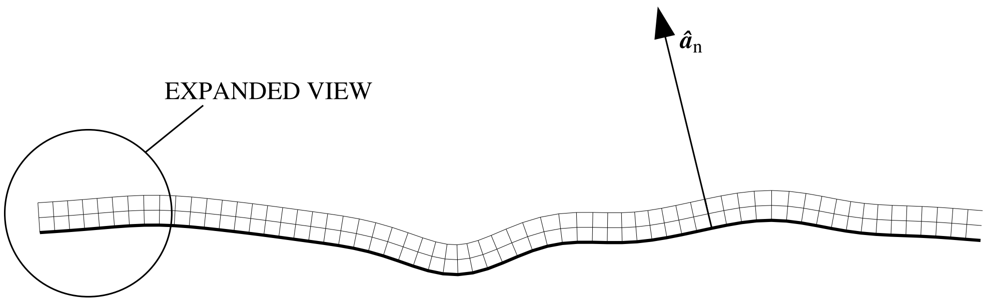

Figure 4: Segment of typical surface and computational mesh.

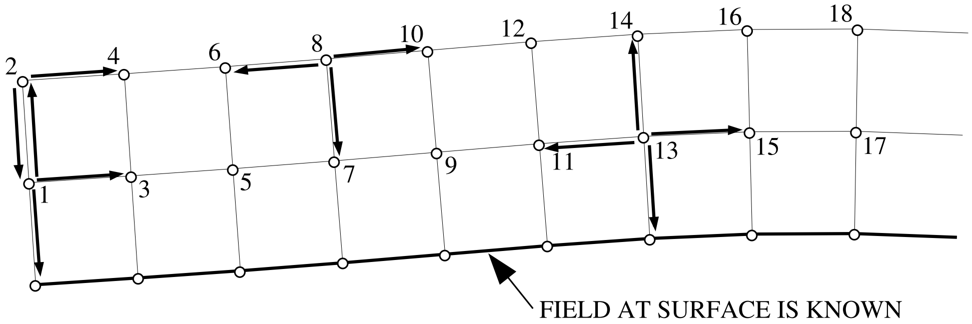

Figure 5: Expanded view of computational mesh.

first and last two nodes are exceptional and must be given special consideration. In our implementation, all odd nodes (except 1 and $N-1$) are connected to neighboring nodes in a manner similar to node 13 shown in Fig. 5. Since neighbors are available above, below, to the left, and to the right, the local polar scheme proposed by Pous can be employed [2]. As mentioned before, this simplifies calculation of the connectivity weights and makes consideration of the singularity in the Green's function at the surface unnecessary. All even nodes between 2 and N are handled using the MEI method. These nodes are connected to one neighbor in the interior and to the neighbors to the left and right as shown for node 8. Nodes 2 and N are both connected to only two neighbors and are handled using the MEI method. Nodes 1 and $N-1$ are treated using the local polar approximation. For these nodes, an additional node is assumed to exist to the left of node 1 or to the right of node $N-1$ so that the proper weights can be determined. However, the field is assumed to be zero at the fictitious neighbor and it does not enter into the calculation. Note that the tapered incident field is small near nodes 1 and $N-1$ so setting the field to zero should introduce negligible error. With this connectivity scheme, the connectivity matrix $\mathbf{A}$ is not only sparse, but is also tightly banded—there are a total of five diagonals (including the main diagonal) that contain non-zero elements. A number of public domain routines exist, such as those in LINPACK [30], that can be used to efficiently invert such a matrix.

In many rough surface scattering problems bistatic results span a range of over 60 dB. For instance, for slightly rough surfaces the coherent specular reflection contains significant energy relative to the incoherent energy found at grazing angles. This dynamic range requires an extremely accurate numerical solution. In previously published results the accuracy of MEI-based solutions was, at most, weakly dependent on the selection of metrons. However, we found that using an initial selection of metrons that are physically unrealizable leads to poor results. Because of the accuracy required and the difficulty in making a "good" initial selection of metrons, an iterative scheme was used. The initial set of metrons was

$$\begin{aligned} J_s^1(\mathbf{r}_i) &= \exp(-x_i^2/g^2) \\ J_s^2(\mathbf{r}_i) &= \cos(k_0\xi_i) \\ J_s^3(\mathbf{r}_i) &= \sin(k_0\xi_i) \\ J_s^4(\mathbf{r}_i) &= \exp(-x_i^2/g^2)\cos(k_0 y_i) \\ J_s^5(\mathbf{r}_i) &= \exp(-x_i^2/g^2)\sin(k_0 y_i) \end{aligned}$$

where g is the taper factor commensurate with the incident field, $\mathbf{r}_i = (x_i, y_i)$ corresponds to the ith point along the surface, ξ_i is the path length along the surface from the first point to the ith point, and k_0 is the free-space wavenumber. Using the following Green's function

$$G(\mathbf{r}|\mathbf{r}') = \frac{k_0\eta_0}{4} H_0^{(2)}(k_0|\mathbf{r}-\mathbf{r}'|), \qquad (21)$$

where η_0 is the characteristic impedance of free space, the measured fields are obtained (see (5)) using

$$E_z^n(\mathbf{r}) \approx \sum_{i=1}^{N} J_s^n(\mathbf{r}_i) G(\mathbf{r}|\mathbf{r}_i)\Delta\xi_i \qquad (22)$$

where $\Delta\xi_i$ is the distance from the ith to the $(i+1)$th point ($\Delta\xi_N$ is set equal to $\Delta\xi_{N-1}$).

The iterative scheme proceeds as follows. The metrons shown above are employed in the MEI method to obtain the fields above the surface. From these fields a surface current is obtained. The calculated current is used to replace one of the metrons. The calculation of fields and currents is repeated except now a different metron is replaced with the calculated current. This is repeated until sufficient accuracy is obtained or there are no more metrons to update. For each iteration, it was found that there is virtually no change in the scattered field in regions where there is significant energy. The iterative scheme is only necessary to obtain improved accuracy where the fields are significantly less than the maximum. There are a myriad of other iterative schemes that could be developed; the one presented here is not necessarily the optimum one. A better initial selection of metrons may have eliminated the need for iteration. However, this scheme does illustrate that an iterative technique can be used when there is little or no *a priori* knowledge of the actual source distribution.

It is worth mentioning that, in principle, an iterative scheme can be done with little additional computational overhead. The majority of CPU time is spent calculating the terms $G(\mathbf{r}|\mathbf{r}_i)$ for pairs of surface and mesh points. In principle, these terms just need to be calculated once (since they depend only on the geometry of the grid) and then multiplied later by the appropriate metrons. However, in practice this requires the storage of $2N^2$ terms, which represents a prohibitive amount of memory for large problems. The code developed for this study was not optimized, and the Green's functions were recalculated for each iteration.

To calculate far-field quantities or to update the metrons in the iterative scheme, it is necessary to obtain the surface currents from the MEI-derived electric field. The currents are found using

$$J_s = \frac{-1}{jk_0\eta_0}\frac{\partial E_z}{\partial n} \tag{23}$$

where n is normal to the surface. Given the mesh structure and the fact that the total field is zero at the surface, the current can be found at a point on the surface using

$$J_s \approx \frac{-1}{jk_0\eta_0}\frac{E_z(\Delta\upsilon)}{\Delta\upsilon} = \frac{-1}{jk_0\eta_0}\frac{(E_z^{\text{mei}}(\Delta\upsilon) + E_z^{\text{inc}}(\Delta\upsilon))}{\Delta\upsilon} \tag{24}$$

where $E_z^{\text{mei}}(\Delta\upsilon)$ is the MEI-derived scattered field at the first mesh point above the surface (i.e., the first point above the surface normal and on the surface normal) and $E^{\text{inc}}(\Delta\upsilon)$ is the known incident field at the same point. However, this is only accurate to order $O(\Delta\upsilon)$. Since the scattered field is available at two mesh points above the surface, the surface current is obtained using second-order forward-differencing. Thus, the normal derivative is found using

$$\frac{\partial E_z}{\partial n} \approx \frac{1}{2\Delta\upsilon}\left(4E_z(\Delta\upsilon) - E_z(2\Delta\upsilon)\right) \tag{25}$$

where $E_z = E_z^{\text{mei}} + E_z^{\text{inc}}$ is the total field.

Our goal is to calculate the bistatic radar cross section per unit length for a plane wave incident on a 1-D surface. This is found using [31]

$$\sigma(\theta_s, \theta_i) = 2\pi\frac{I_s\rho}{I_i L} \tag{26}$$

where ρ is the distance to the far-field observation point, L is the length of the surface, I_s is the scattered intensity, I_i is the incident intensity, θ_s is the angle of observation measured from the vertical, and θ_i is the angle of incidence measured from the vertical. In order to find the bistatic radar cross section, it is necessary to convert the surface current to the electric field in the far field. Equation (22) could be used; however, given the distant location of the observation point, the large argument approximation of the Hankel function is used. Thus, for an incident field with unit magnitude, we obtain the cross section using

$$\sigma(\theta_s, \theta_i) = \frac{k_0}{4}\left|\sum_{i=1}^{N} J_s(\mathbf{r}_i)\Delta\xi_i exp(jk_0(x_i\cos\theta_s + y_i\sin\theta_s))\right|^2. \tag{27}$$

V. Results

To illustrate the results of the method, consider a surface with $k_0h = 0.33$ and $k_0l = 2.83$. This surface has an RMS slope angle of $\gamma = 9.46°$. Fifty surface realizations of length $L = 80\lambda$ were generated and enclosed in a mesh with $\Delta x = \Delta\upsilon = \lambda/16$. (This mesh spacing is typical of that reported in other applications of the MEI method. It was found that using a finer spacing did not improve the results, while a coarser mesh yielded slightly worse results.) Figure 6 shows the bistatic radar cross section obtained using the MEI method and an FDTD technique [32] that is known to be accurate for this type of surface. Since normal incidence was used, coherent specular return is at 0°. The small oscillations in the curve are due to the use of a finite number of surface realizations. Since two different sets of surface realizations were used, the oscillations do not coincide. These two methods show excellent agreement throughout the 60 dB range of the results. The MEI method results were obtained after three iterations of the metrons.

Figure 7 shows the cross section when the same surface as used for the results in Fig. 6 is illuminated by a wave incident at 45°. All aspects of the calculation (e.g., mesh structure, taper factor, and surface realizations) are the same as before except five iterations were used. As expected, the coherent specular peak is at 45°. The two results show excellent agreement everywhere except toward backward grazing angles.

Figure 8 shows the results for a surface with $k_0h = 1.72$ and $k_0l = 7.31$ that is illuminated with a normally incident wave. Five iterations were used. Compared to the previous surface, the correlation length has increased by a factor of $2\frac{7}{12}$ and the RMS surface height has increased by twice this same factor. This change in parameters approximately doubles the RMS slope angle so that it is now 18.43°. Because this surface is fairly rough, it produces no clear specular return; instead incoherent energy is broadly distributed over a range of scattering angles.

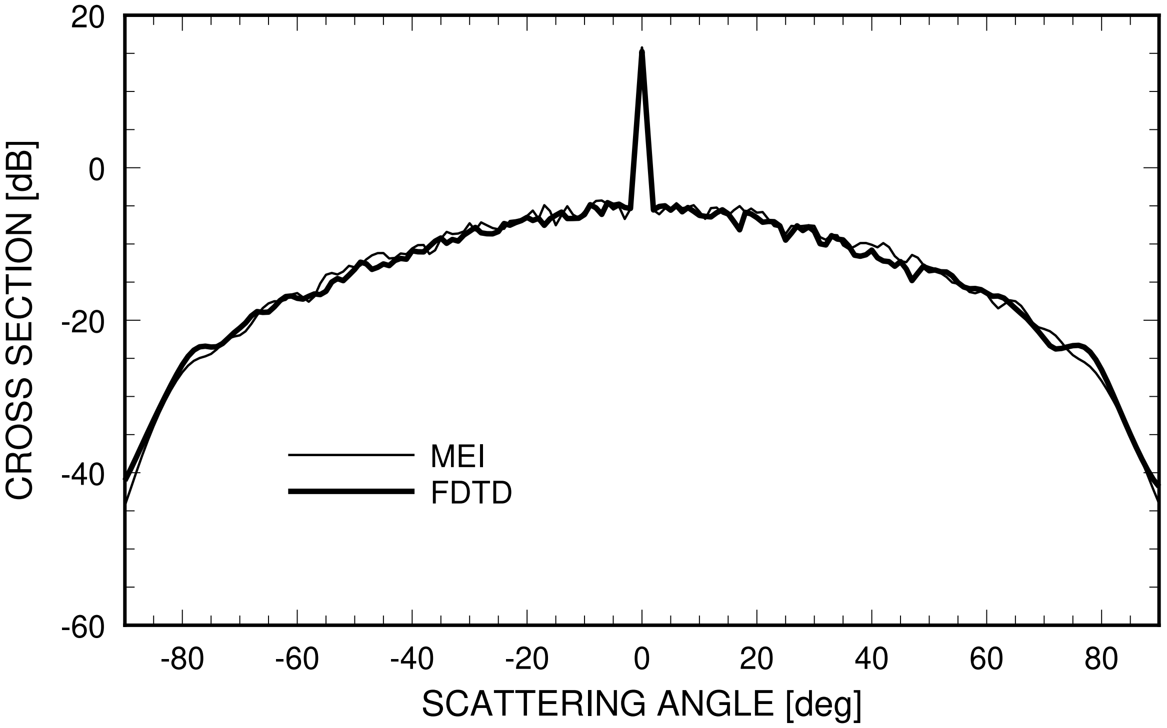

Figure 6: Radar cross section as a function of scattered angle for normal illumination of a surface with $k_0h = 0.33$ and $k_0l = 2.83$.

Again, there is good agreement between the two methods except at low grazing angles where the MEI method overpredicts the cross section.

The three results presented here were done in a consistent manner, i.e., all were solved using the same approach. The only difference between runs was the number of iterations—no other modifications were attempted to try to optimize the results for a particular geometry. In fact, there is every reason to believe that the results presented here are not optimum. For example, a better metron for use in the initial set might be one obtained from the physical optics equivalent, namely, $\mathbf{J}_s \approx 2\mathbf{n} \times \mathbf{H}^{\text{inc}}$. This could be used instead of the constant metron J_s^1 given in (21) and probably would be appropriate for surfaces with relatively long correlation lengths. Additionally, by incorporating the x and y components of the wavenumber rather than just using k_0, the metrons could contain more knowledge of the incident field. There may also be better mesh structures than the one presented here.

V. Conclusions

Although the limits of the MEI method have not been completely explored, the work presented in this paper illustrates that the method has the potential to provide accurate solutions to rough surface scattering problems. The problem examined in this study required a large dynamic range. Accuracy was achieved using an iterative scheme. Additional accuracy was obtained by calculating the surface currents using second-order forward differencing.

Since the MEI method provides a solution via a sparse and relatively small matrix, it can potentially solve rough surface scattering problems in three dimensions. In that case the metrons would be a function of two variables, rather than one, and it may be much harder to select "good" metrons. Therefore, the use of an iterative scheme in three dimensions may be critical for successful implementation.

The TE problem has not been discussed but is solved in a manner very similar to that presented here. The solution for penetrable objects involves enclosing the material

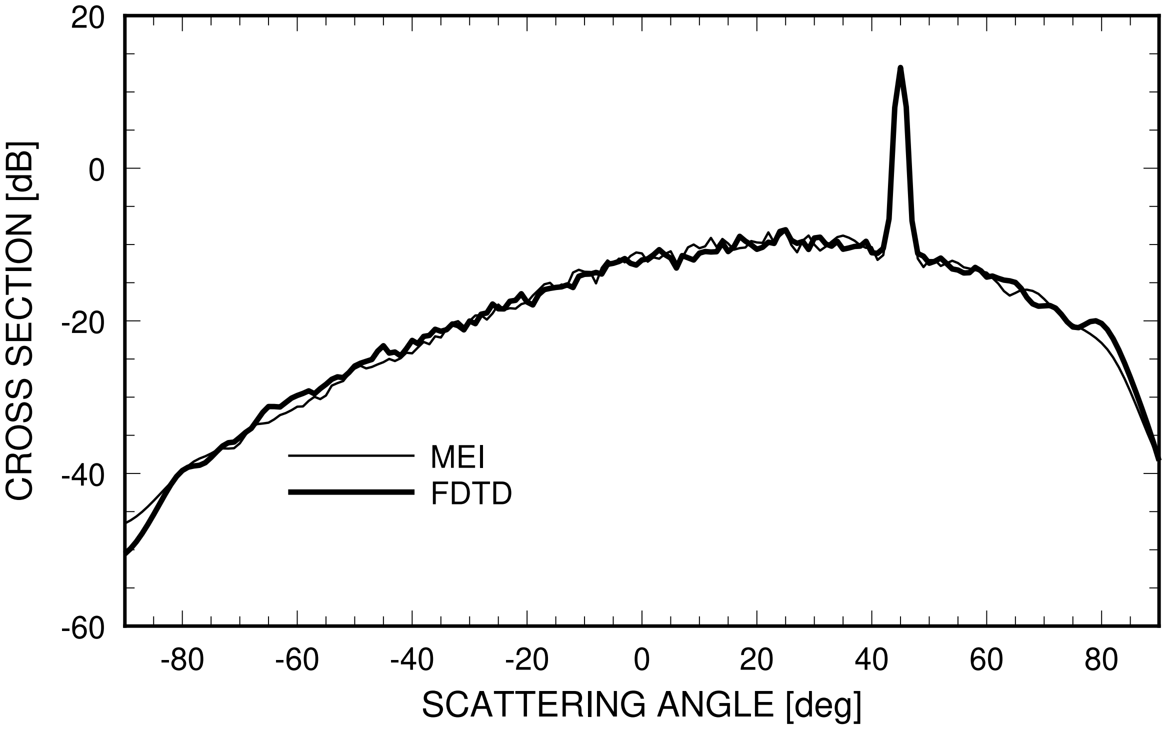

Figure 7: Radar cross section as a function of scattered angle when $\theta_i = 45^\circ$ for a surface with $k_0 h = 0.33$ and $k_0 l = 2.83$.

interface in a mesh—with mesh points on both sides of the interface. This mesh can be terminated close to the interface, but the solution is complicated by the fact that metrons must be specified in terms of both their value at the surface and their normal derivative at the surface.

Several other problems remain to be investigated. For example, if a surface is extremely rough, the computational mesh may cross itself. In other words, as mesh points are placed along the surface normal, some points will no longer have monotonically increasing values in the x direction if the normal directions change too abruptly (such as in a narrow valley). This type of highly distorted mesh does not permit use of the local polar approximation but may yield to analysis by using the MEI method for nodes in the vicinity of the mesh overlap. Other remaining topics include determination of optimum mesh structure (both in terms of spacing and number of layers) and best selection of metrons.

Acknowledgements

This work was supported by the Office of Naval Research, Code 321OA, and by the National Science Foundation under Grant No. ECS-9253547 .

References

[1] K.K. Mei, R. Pous, Z. Chen, and Y. Liu. Measured Equation of Invariance: A New Concept in Field Computation. In 1992 IEEE AP-S International Symposium and URSI Radio Science Meeting Digest, page 544, Chicago, IL, July 1992.

[2] R. Pous. *The Measured Equation of Invariance: A New Concept in Field Computation.* PhD thesis, University of California, Berkeley, CA, 1992.

[3] M.D. Prouty, K.K. Mei, S.E. Schwarz, and R. Pous. A New Approach to Quasi-Static Analysis with Application to Microstrip. *IEEE Microwave and Guided Wave Letters*, 3(9):302–304, 1993.

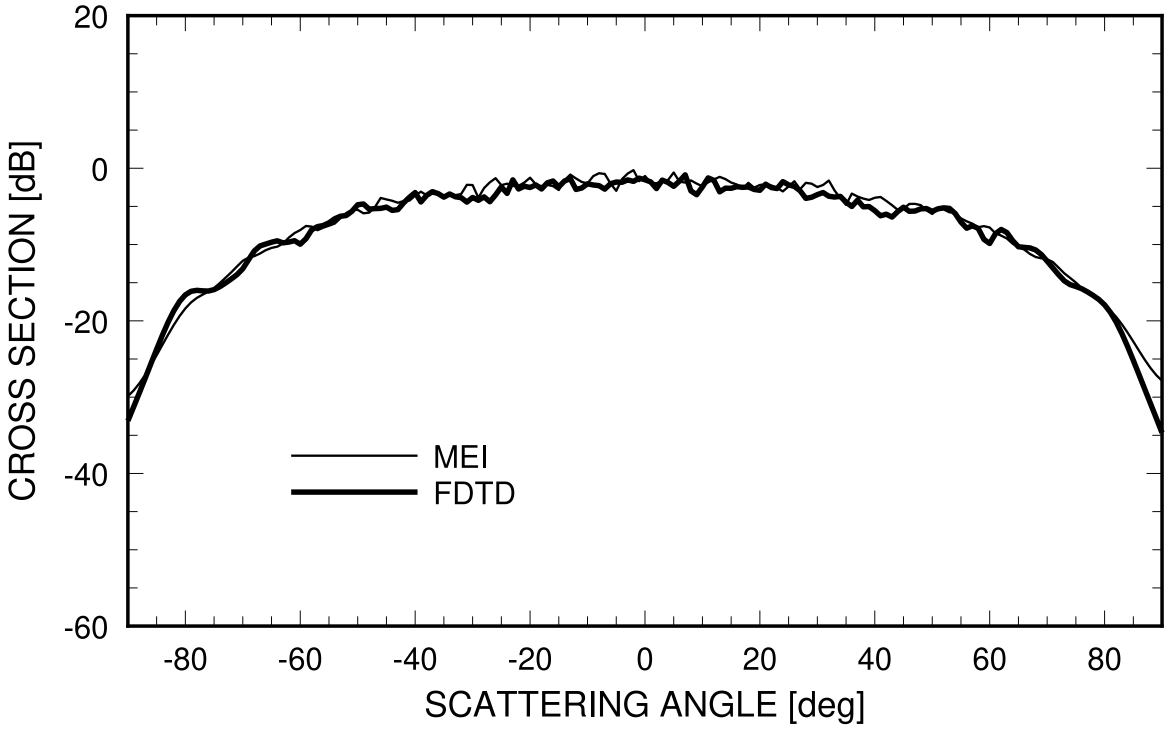

Figure 8: Radar cross section as a function of scattered angle for normal illumination of a surface with $k_0h = 1.72$ and $k_0l = 7.31$.

[4] K.K. Mei, R. Pous, Z. Chen, Y.W. Liu, and M.D. Prouty. Measured Equation of Invariance: A New Concept in Field Computation. *IEEE Trans. Antennas Propagat.*, 42(3):320–328, 1994.

[5] A.C. Cangellaris and D.B. Wright. Application of the Measured Equation of Invariance to Electromagnetic Scattering by Penetrable Bodies. *IEEE Trans. Mag.*, 29(2):1628–1631, 1993.

[6] D.B. Wright and A.C. Cangellaris. MEI-Based Mesh Truncation Conditions for the Finite-Element Modeling of EM scattering by Two-Dimensional Penetrable Targets. In 1993 IEEE AP-S International Symposium and URSI Radio Science Meeting, Ann Arbor, MI, June 1993.

[7] Y. Li, Z.J. Cendes, and X. Yuan. A Modified MEI Method for Solving Scattering Problems with the Finite Element Method. In 1993 IEEE AP-S International Symposium and URSI Radio Science Meeting, Ann Arbor, MI, June 1993.

[8] T.L. Barkdoll and R. Lee. Finite Element Analysis of Bodies of Revolution Using the Measured Equation of Invariance. In 1993 IEEE AP-S International Symposium and URSI Radio Science Meeting, Ann Arbor, MI, June 1993.

[9] J.L. Young, J.B. Schneider, and R.G. Olsen. Laplace's Equation and the Measured Equation of Invariance. In COMPUMAG Conference on the Computation of Electromagnetic Fields, Miami, Florida, November 1993.

[10] A.G. Voronovich. Small-Slope Approximation in Wave Scattering by Rough Surfaces. *Sov. Phys. JETP*, 62(1):65–70, 1985.

[11] S.L. Broschat and E.I. Thorsos. A Numerical Study of the Small Slope Approximation for Rough Surface Scattering. In Topical Meeting of the ICO, Atmospheric, Volume, and Surface Scattering and Propagation, Florence, Italy, 1991.

[12] E.I.Thorsos and S.L. Broschat. An Investigation of the Small Slope Approximation for Scattering from Rough Surfaces: Part I—Theory. *J. Acoust. Soc. Am.*, 97(3), 1995.

[13] D. Winebrenner and A. Ishimaru. Investigation of a Surface Field Phase Perturbation Technique for Scattering from Rough Surfaces. *Radio Sci.*, 20:161–170, 1985.

[14] R.M. Fitzgerald and A.A. Maradudin. A Reciprocal Phase-Perturbation Theory for Rough-Surface Scattering. *Waves in Random Media*, 4:275–296, 1994.

[15] D.M. Milder. An Improved Formalism for Wave Scattering from Rough Surfaces. *J. Acoust. Soc. Am.*, 89(2):529–541, 1991.

[16] P.J. Kaczkowski and E.I. Thorsos. Application of the Operator Expansion Method to Scattering from One-Dimensional Moderately Rough Dirichlet Random Surfaces. *J. Acoust. Soc. Am.*, 96(2):957–972, 1994.

[17] R. Dashen and D. Wurmser. Approximate Representation of the Scattering Amplitude. *J. Math. Phys.*, 32:986–996, 1991.

[18] E. Rodriguez and Y. Kim. A Unified Perturbation Expansion for Surface Scattering. *Radio Sci.*, 27:79–93, 1992.

[19] E. Rodriguez, Y. Kim, and S.L. Durden. A Numerical Assessment of Rough Surface Scattering Theories: Horizontal Polarization. *Radio Sci.*, 27:497–513, 1992.

[20] V.I. Tatarskii. The Expansion of the Kirchoff Approximation for Rough Surface Scattering Using a Gaussian Roughness Spectrum. *Wave in Random Media*, 3:127–146, 1993.

[21] E.I. Thorsos. The Validity of the Kirchhoff Approximation for Rough Surface Scattering Using a Gaussian Roughness Spectrum. *J. Acoust. Soc. Am.*, 83:78–92, 1988.

[22] H.L. Chan and A.K. Fung. A Numerical Study of the Kirchhoff Approximation in Horizontally Polarized Backscattering from a Random Surface. *Radio Sci.*, 13(5):811–818, 1978.

[23] S.H. Lou, L. Tsang, and C.H. Chan. Application of the Finite Element Method to Monte Carlo Simulations of Scattering of Waves by Random Rough Surfaces: Penetrable Case. *Waves in Random Media*, 1:287–307, 1991.

[24] A.K. Fung, M.R. Shah, and S. Tjuatja. Numerical Simulation of Scattering from Three-Dimensional Randomly Rough Surfaces. *IEEE Trans. Geosci. Remote Sensing*, 32(5):986–994, 1994.

[25] C.H. Chan, S.H. Lou, L. Tsang, and J.A. Kong. Electromagnetic Scattering of Waves by Rough Surfaces: A Finite-Difference Time-Domain Approach. *Microwave Opt. Technol. Lett.*, 4(9):355–359, 1991.

[26] F.D. Hastings, S.L. Broschat, and J.B. Schneider. An Application of the Contour Path Finite-Difference Time-Domain Method to Rough Surface Scattering. In 1993 IEEE AP-S International Symposium and URSI Radio Science Meeting, Ann Arbor, MI, June 1993.

[27] J.A. Ogilvy. *Theory of Wave Scattering from Random Rough Surfaces.* Adam Hilger, Bristol, England, 1991.

[28] E.I. Thorsos. The Validity of the Perturbation Approximation for Rough Surface Scattering Using a Gaussian Roughness Spectrum. *J. Acoust. Soc. Am.*, 86:261–277, 1989.

[29] S.L. Broschat, E.I. Thorsos, and A. Ishimaru. The Phase Perturbation Technique vs an Exact Numerical Method for Random Rough Surface Scattering. *J. Electromagnetic Waves Applications*, 3(3):237–256, 1989.

[30] J.J. Dongarra, C.B. Moler, J.R. Bunch, and G.W. Stewart. *LINPACK User's Guide.* Society for Industrial and Applied Mathematics, Philadelphia, PA, 1979.

[31] A. Ishimaru. *Wave Propagation and Scattering in Random Media.* Academic, New York, 1978.

[32] F.D. Hastings, J.B. Schneider, and S.L. Broschat. A Monte Carlo Contour Path FDTD Technique for Rough Surface Scattering. Submitted to *IEEE Trans. Antennas Propagat.*, 1994.